Isolation and characterization of mutants defective in the localization of LCIB, an essential factor for the carbon-concentrating mechanism in Chlamydomonas reinhardtii.

AUTHOR(S):

Yamano, Takashi; Asada, Atsuko; Sato, Emi; Fukuzawa, Hideya

Title:

Isolation and characterization of mutants defective in the localization of LCIB, an essential factor for the CO_2-concentrating mechanism in *Chlamydomonas reinhardtii*

Authors:

Takashi Yamano, Atsuko Asada, Emi Sato, Hideya Fukuzawa

Graduate School of Biostudies, Kyoto University, Kyoto, 606-8502, Japan

Corresponding Author:

Hideya Fukuzawa

Graduate School of Biostudies, Kyoto University, Kyoto, 606-8502, Japan

Phone: +81-75-753-6391

FAX: +81-75-753-6127

E-mail: fukuzawa@lif.kyoto-u.ac.jp

Abstract

The unicellular green alga *Chlamydomonas reinhardtii* acclimates to low-CO_2 (LC) conditions by actively transporting inorganic carbon (Ci) into the cell, resulting in an increase in photosynthetic efficiency. This mechanism is called the CO_2-concentrating mechanism (CCM), and soluble protein LCIB is essential for the CCM. LCIB is localized in the vicinity of pyrenoid, a prominent structure in the chloroplast, under LC conditions in the light. In contrast, in the dark or in high-CO_2 (HC) conditions, where the CCM is inactive, LCIB diffuses away from the pyrenoid. Although the functional importance of LCIB for the CCM has been shown, the significance and mechanism of the change in suborganellar localization of LCIB remain to be elucidated. In this study, we screened 13,000 DNA-tagged mutants and isolated twelve aberrant LCIB localization (*abl*) mutants under LC conditions. *abl-1* and *abl-3* with dispersed and speckled localization of LCIB in the chloroplast showed significant decreases in Ci affinity, Ci accumulation, and CO_2 fixation, suggesting two possibilities: a mutation in a gene essential for the CCM caused by DNA-tagging could cause the dispersed and speckled LCIB localization, or the dispersed and speckled LCIB localization itself could cause the dysfunction of the CCM. Ten *abl* mutants (*abl-1*, *abl-3*, *abl-4*, *abl-5*, *abl-6*, *abl-7*, *abl-8*, *abl-9*, *abl-11*, and *abl-12*) showed not only aberrant LCIB localization but also reduced pyrenoid sizes. Moreover, three *abl* mutants (*abl-10*, *abl-11*, and *abl-12*) showed increased numbers of pyrenoids per cell. These results suggested that the specific LCIB localization could be related to pyrenoid development.

Keywords

Chlamydomonas reinhardtii, CO_2-concentrating mechanism, LCIB, pyrenoid

Introduction

Some aquatic photosynthetic organisms possess a CO_2-concentrating mechanism (CCM) to maintain optimal photosynthetic activity under CO_2-limiting conditions caused by the slow diffusion rate of CO_2 in aquatic environments and the low catalytic capacity of ribulose 1, 5-bisphosphate carboxylase-oxygenase (Rubisco) – the CO_2 fixation enzyme. In *Chlamydomonas reinhardtii*, a single cell green alga, the CCM operates by inducing numerous CCM-related proteins involved in acquiring dissolved inorganic carbon (Ci; CO_2 and HCO_3^-) from external sources and generating elevated levels of HCO_3^- in the stroma (Moroney and Ynalvez 2007).

Previously, we identified low-CO_2 (LC)-inducible genes *LCIB* and *LCIC* encoding chloroplast-targeted soluble proteins (Miura et al. 2004). Recently, LCIB was shown to be essential for the operation of the CCM by characterization of the high-CO_2 (HC)-requiring mutant *ad-1* (Wang et al. 2006; Duanmu et al. 2009). LCIB interacts with its homologous protein LCIC *in vivo* and they co-localize in the vicinity of pyrenoid, a prominent structure in the chloroplast, under LC conditions (Yamano et al. 2010). In contrast, when LC-acclimated cells were transferred to dark or HC conditions, where the CCM is switched off and the LCIB/LCIC complex diffuses away from the pyrenoid. Although the functional importance of LCIB for the CCM has been shown, the significance and mechanism of the change in suborganellar localization of LCIB remain to be elucidated.

In this study, to investigate the mechanism of light- and CO_2-dependent LCIB localization and the relationship between specific LCIB localization and operation of the CCM, we isolated and characterized mutants showing aberrant LCIB localization (*abl*). The CCM was defective in mutants showing dispersed and speckled localization

of LCIB in the chloroplast. Moreover, most mutants showed abnormal pyrenoid development with reduced sizes or increase of numbers of pyrenoids, suggesting that specific LCIB localization could be related to normal pyrenoid development.

Materials and methods

Strains and culture conditions

C. reinhardtii strain 5D *(nit1-305, cw15, mt−)* was transformed with a plasmid expressing GFP-fused LCIB constitutively (Yamano et al. 2010), and the obtaining transformant showed bright GFP fluorescence was used as a host strain for transformation. For maintenance, cells were cultured in Tris-acetate-phosphate (TAP) medium, and for photoautotrophic growth, cells were cultured in a modified high-salt medium (HSM) containing 20 mM MOPS aerated with air enriched with 5% CO_2 (HC conditions) or ordinary air containing 0.04% CO_2 (LC conditions) at 25°C under continuous illumination at 80 μmol photons m^{-2} s^{-1}.

Transformation of cells

A 1,999 bp DNA fragment containing the hygromycin (hyg)-resistant gene *aph7"* was amplified by PCR from plasmid pHyg3 (Berthold et al. 2002) using PrimeSTAR GXL DNA Polymerase (TAKARA BIO, Shiga, Japan) by 35 cycles of denaturation for 10 sec at 98°C, annealing for 15 sec at 60°C, and extension for 2 min at 68°C with a forward primer (5'-GCACCCCAGGCTTTACACTTTATGCTTCC-3') and reverse primer (5'-CCATTCAGGCTGCGCAACTGTTGG-3'). The PCR product was purified using a PCR purification kit (QIAGEN, Valencia, CA, USA) and the concentration was adjusted to 100 μg mL^{-1}.

Transformation of *C. reinhardtii* cells was performed as reported previously (Yamano et al. 2013). Briefly, host strain cells in early logarithmic phase were collected and transformed by electroporation using a NEPA21 electroporator (NEPAGENE, Chiba, Japan). The transformants were incubated at 25°C for 24 h with gentle agitation under illumination at 1.5 μmol photons m^{-2} s^{-1} and then screened on TAP plates containing 30 μg mL^{-1} hygromycin at 25°C under 80 μmol photons m^{-2} s^{-1}. After 4 days, colonies of transformants appeared and then subjected to the screening process for the identification of mutants.

Screening of aberrant LCIB localization mutants

Hyg-resistant transformants cultured in 96-well mictrotiter plates were grown in a chamber supplied with HC for 12 h and then shifted in a chamber supplied with LC air for CCM induction. Fluorescence images derived from LCIB-GFP in each transformant was observed by fluorescence microscopy using an Axioskop 2 (Zeiss, Oberkochen, Germany), and mutants showing aberrant LCIB localization were screened. To obtain high-resolution fluorescence images, mutants were observed by confocal fluorescence microscopy using a TCS SP8 (Leica, Wetzlar, Germany), and the obtained images were deconvoluted using the Huygens Essential software (Scientific Volume Imaging B.V., Hilversum, The Netherlands).

Measurement of inorganic carbon-dependent photosynthetic oxygen evolution

The affinity for Ci was evaluated by measuring the rate of dissolved Ci-dependent photosynthetic oxygen (O_2) evolution. Cells were collected by centrifugation and then resuspended in Ci-depleted 50 mM HEPES-KOH buffer (pH 7.8) at 15 μg mL^{-1}

chlorophyll. Photosynthetic O_2 evolution was measured using a Clark-type oxygen electrode (Hansatech Instruments, King's Lynn, UK) as described previously (Yamano et al. 2008). The maximum O_2-evolving activity, defined as V_{max}, was measured in the presence of 10 mM $NaHCO_3$.

Measurement of intercellular concentration of dissolved inorganic carbon

The intercellular concentration of dissolved Ci was measured by the silicone oil centrifugation method as described previously (Ohnishi et al. 2010). Cells grown under LC conditions were collected by centrifugation at 600 *g*, then suspended at a cell density of approximately 25 μg mL^{-1} chlorophyll in Ci-depleted 50 mM HEPES-NaOH buffer (pH 7.8), and 1.2 mL of the cell suspension was bubbled with N_2 gas for 10 min in an O_2 electrode. First, a 60 μL silicone oil layer (SH550:SH556 = 4:7 [v/v]) was overlaid on a 20 μL layer of the termination solution containing 1 M glycine-NaOH, pH 10.0, and 0.75% sodium dodecylsulfate (SDS; w/v). Then, 300 μL of the cell suspension were further overlaid on the silicone oil layer. Ci uptake was initiated by the addition of 10 μL of $NaH^{14}CO_3$ at 100 μM concentration, which was immediately followed by 80 s of illumination with an actinic light source of 300 μmol photons m^{-2} s^{-1}, and the reaction was terminated by centrifugation. After centrifugation, the labeled cells were immediately frozen using liquid nitrogen and then suspended in 400 μL of 0.1 N NaOH. The alkaline cell suspension was divided into two 160 μL aliquots. One was directly subjected to liquid scintillation counting, which was described as total Ci uptake. The other aliquot was added to 200 μL of 0.5 N HCl, desiccated to liberate ^{14}C except for the fixed $^{14}CO_2$, suspended with 200 μL of water, and then subjected to a liquid scintillation counting to analyze the ^{14}C level, which was described as CO_2

fixation. Ci accumulation was calculated as the difference between the total Ci uptake and CO_2 fixation. Each value was corrected by estimating the cell volume as sorbitol impermeable space (SIS) using [^{14}C]sorbitol and $^{3}H_2O$ as described previously (Heldt 1980).

Immunoblotting analysis

Extracted soluble proteins suspended in SDS gel-loading buffer containing 50 mM Tris-HCl (pH 8.0), 25% glycerol (w/v), 2% SDS, and 0.1 M DTT were incubated at 65°C for 10 min and subsequently centrifuged at 14,000 g for 3 min. The supernatant containing solubilized proteins was subjected to SDS-PAGE analysis. After electrophoresis, proteins were electrophoretically transferred to polyvinylidene difluoride membranes (Bio-Rad, Hercules, CA, USA). Membranes were blocked with 5% (w/v) non-fat skim milk (Wako, Osaka, Japan) in phosphate-buffered saline (PBS). Blocked membranes were washed with PBS containing 0.1% (v/v) Tween-20 (PBS-T) and treated with an anti-LCIB antibody (1:5,000 dilution) in PBS-T. A horseradish peroxidase-conjugated goat anti-rabbit IgG antibody (1:10,000 dilution; GE Healthcare, Milwaukee, WI, USA) was used as a secondary antibody. Immunologically positive signals were visualized using Luminata Crescendo Western HPR substrate (Millipore, Billerica, MA, USA) and detected using an ImageQuant LAS 4000 (Fuji Film, Tokyo, Japan).

Results

Effect of cycloheximide on the accumulation and localization of LCIB

As reported previously (Yamano et al. 2010), LCIB-GFP signals were observed as a

ring-like structure in the vicinity of the pyrenoid, and within 1 h after transfer to LC-dark conditions, the signals diffused from the pyrenoid throughout the entire chloroplast and aggregated into punctuate structures (Fig. 1A). To determine whether this change in LCIB localization is associated with *de novo* protein synthesis, the effect of cycloheximide (CHX), which inhibits the *de novo* protein synthesis, on LCIB accumulation was examined under LC-light and LC-dark conditions (Fig. 1B and 1C). Accumulation of endogenous LCIB was induced by shifting from HC (lane 1) to LC conditions (lanes 2 to 5), and this accumulation was inhibited by addition of CHX (lane 6). In contrast, the level of exogenous LCIB-GFP was constitutive because of the operation of the constitutive promoter expressing LCIB-GFP (lanes 1 to 6). The accumulation levels of both endogenous LCIB and exogenous LCIB-GFP were not significantly altered during the localization changes or by the addition of CHX (lanes 7 to 11). Moreover, addition of CHX to the culture medium inhibited the re-accumulation of LCIB in the vicinity of pyrenoid after a switch from LC-dark to LC-light conditions (Fig. 1D). These results suggested that the change in LCIB localization is not associated with *de novo* synthesis of LCIB itself, and additional factor(s) other than LCIB, which is translated after shifting the culture conditions from dark to light, could be needed for the change in LCIB localization.

Screening for aberrant LCIB localization mutants

To identify factors responsible for the change in LCIB localization and to understand the mechanism of the regulation in the response to light and CO_2 conditions, *abl* mutants were screened for among hyg-resistant transformants (Fig. 2). First, to construct insertion mutant libraries, a 1,999 bp DNA fragment containing the hyg

resistance gene *aph7"* was amplified by PCR, and the host strain expressing LCIB-GFP was transformed with the PCR products. In total, approximately 13,000 transformants were generated. Each transformant was cultured under LC conditions, and the fluorescence signals derived from LCIB-GFP were observed individually using fluorescence microscopy. As a result, 12 strains were isolated as *abl* mutants.

Next, LCIB localization under LC conditions was examined in detail using confocal fluorescence microscopy (Fig. 3). In host stain cells, as shown in a previous report (Yamano et al. 2010), the fluorescence signals of LCIB-GFP at the basal region of the chloroplast were observed as tubule-like structures in the pyrenoid as well as a ring-like structure around the pyrenoid. Some thylakoids penetrate the pyrenoid, which are termed pyrenoid tubules (Ohad et al. 1967); therefore, LCIB in the pyrenoid could be localized along the pyrenoid tubules.

In mutants *abl-1* and *abl-3*, dispersed and speckled fluorescence signals were observed in the chloroplast. Occasionally, two or more pyrenoids were observed in *abl-3*. In *abl-2*, fluorescence signals were observed as a ring structure as shown in the host strain cells, but LCIB-GFP localization was detected at the apical side of the chloroplast. This mislocalization of LCIB-GFP could be caused by abnormal localization of the pyrenoid in the chloroplast. In other mutants, typical fluorescence signals were observed in the basal regions (*abl-4* and *abl-9*), apical regions (*abl-5* and *abl-8*), or lateral regions (*abl-6* and *abl-7*) of chloroplasts as an incomplete ring or aggregated structures. In mutant *abl-11*, fluorescence signals were dispersed and partially aggregated, but not speckled as in *abl-1* and *abl-3*. In *abl-10* and *abl-12*, two or more pyrenoids were observed in the chloroplast, and aggregated fluorescence signals were observed in the vicinity of the pyrenoids, forming incomplete ring structures. We

also performed indirect immunofluorescence assays using anti-LCIB and anti-LCIC antibodies and confirmed that endogenous LCIB and LCIC were also mislocalized in all *abl* mutants (Online resource 1).

Abnormal pyrenoid development in abl mutants

To investigate the relationship of pyrenoid development and proper LCIB localization, the pyrenoid sizes of *abl* mutants under LC conditions were compared to that of the host stain (Fig. 4A). In host strain cells, the pyrenoid developed under LC conditions and its size increased from 2.52 μm^2 to 4.96 μm^2 (1.96-fold). The pyrenoid sizes of LC-grown *abl-2* and *abl-10* were not significantly different from that of LC-grown host strain. In contrast, other *abl* mutants grown under LC conditions showed significantly decreased pyrenoid sizes compared with LC-grown host strain cells, and these sizes were equivalent to that of HC-grown host strain cells, suggesting that pyrenoid development was defective in these mutants.

Because more than one pyrenoid was observed in the chloroplast in *abl-10*, *abl-11*, and *abl-12* (Fig. 3), actual numbers of pyrenoids per cell were counted (Fig. 4B and C). The average numbers of pyrenoids per single host strain, *abl-10*, *abl-11*, and *abl-12* cell were 1.0 ± 0.0, 3.3 ± 1.2, 1.9 ± 0.7, and 4.6 ± 1.9, respectively.

Photosynthetic characteristics of abl mutants

To evaluate the photosynthetic characteristics of the obtained mutants, the rates of photosynthetic O_2 evolution under changing external Ci concentrations were measured (Table 1). Under LC conditions, mutants *abl-1* and *abl-3* showed much higher photosynthetic $K_{0.5}$ (Ci) values of 281.6 µM and 670.5 µM, respectively, compared with

a host strain value of 50.7 μM, indicating that photosynthetic affinity for Ci was drastically decreased in the mutants. To further evaluate the effect of LCIB mislocalization in *abl-1* and *abl-3*, the accumulation and fixation of [^{14}C]-labeled Ci was measured (Fig. 5). Mutants *abl-1* and *abl-3* showed significantly decreased Ci accumulation of 0.62 mM (41% of host strain) and 0.39 mM (26% of host strain) and of CO_2 fixation at 0.53 nmol μL SIS^{-1} (37%) and 0.29 (21%) nmol μL SIS^{-1}, respectively.

Discussion

In this study, to investigate the mechanism of light- and CO_2-dependent LCIB localization and the relationship between the specific LCIB localization and functioning of the CCM, we isolated and characterized 12 mutants with abnormal LCIB localization. LCIB is an essential factor for in the CCM that changes its localization in response to light as well as CO_2 concentration, and its change in localization may be associated with the operation of the CCM (Duanmu et al. 2009; Yamano et al. 2010). Therefore, characterization of these mutants could lead to a better understanding of the switching mechanism between activation and inactivation of the CCM.

As a result of high-resolution observation of fluorescence signals, aberrant LCIB-GFP localization could be categorized into at least five types; Type A, dispersed and speckled localization in the chloroplast (*abl-1* and *abl-3*); Type B, dispersed and partially aggregated localization in the chloroplast (*abl-11*); Type C, aggregated localization in a specific region of the chloroplast (*abl-4*, *abl-5*, *abl-6*, *abl-7*, *abl-8*, and *abl-9*); Type D, localization in the vicinity of a mislocalized pyrenoid (*abl-2*); and Type E, localization in the vicinity of two or more pyrenoids (*abl-10* and *abl-12*). Among these, only Type A mutants showed decreased CCM activity (Table 1 and Fig. 5),

raising two possibilities. One is that the mutation in a gene essential for the CCM caused by DNA-tagging could cause dispersed and speckled localization of LCIB. The other is that the dispersed and speckled localization of LCIB itself could cause the dysfunction of the CCM. Furthermore, considering that Type B–E mutants did not showed significant decreases in Ci affinity under LC conditions (Table 1), it was also speculated that as long as LCIB is aggregated in the chloroplast, LCIB could function as a CCM component, and the functional localization of LCIB is not limited to only the vicinity of the basal position of the pyrenoid.

Acknowledgments

We thank Ms. Hiro Iguchi for technical assistance. This work was supported by Japan Society for the Promotion of Science (JSPS) KAKENHI (Grant numbers 23120514, 22380059, and 25120714 to H.F., and 25840109 to T.Y.), JST, and ALCA.

References

Berthold P, Schmitt R, Mages W (2002) An engineered *Streptomyces hygroscopicus aph 7″* gene mediates dominant resistance against hygromycin B in *Chlamydomonas reinhardtii*. Protist 153:401–412

Duanmu D, Wang Y, Spalding MH (2009) Thylakoid lumen carbonic anhydrase (CAH3) mutation suppresses air-Dier phenotype of LCIB mutant in *Chlamydomonas reinhardtii.* Plant Physiol 149:929–937

Heldt HW (1980) Measurement of metabolite movement across the envelope and of the pH in the stroma and the thylakoid space in intact chloroplasts. Methods Enzymol 69:604–613

Miura K, Yamano T, Yoshioka S, Kohinata T, Inoue Y, Taniguchi F, Asamizu E, Nakamura Y, Tabata S, Yamato KT, Ohyama K, Fukuzawa H (2004) Expression profiling-based identification of CO_2-responsive genes regulated by CCM1 controlling a carbon-concentrating mechanism in *Chlamydomonas*. Plant Physiol 135:1595–1607

Moroney JV, Ynalvez R (2007) Proposed carbon dioxide concentrating mechanism in *Chlamydomonas reinhardtii*. Eukaryot Cell 6:1251–1259

Ohad I, Siekevitz P, Palade GE (1967) Biogenesis of chloroplast membranes. I. Plastid dedifferentiation in a dark-grown algal mutant (*Chlamydomonas reinhardi*). J Cell Biol 35:521–552

Ohnishi N, Mukherjee B, Tsujikawa T, Yanase M, Nakano H, Moroney JV, Fukuzawa H (2010) Expression of a low CO_2-inducible protein, LCI1, increases inorganic carbon uptake in the green alga *Chlamydomonas reinhardtii*. Plant Cell 22:3105–3117

Wang Y, Spalding MH (2006) An inorganic carbon transport system responsible for

acclimation specific to air levels of CO_2 in *Chlamydomonas reinhardtii*. Proc Natl Acad Sci USA 103:10110–10115

Yamano T, Miura K, Fukuzawa H (2008) Expression analysis of genes associated with the induction of the carbon-concentrating mechanism in *Chlamydomonas reinhardtii*. Plant Physiol 147:340–354

Yamano T, Tsujikawa T, Hatano K, Ozawa S, Takahashi Y, Fukuzawa H (2010) Light and low-CO_2-dependent LCIB-LCIC complex localization in the chloroplast supports the carbon-concentrating mechanism in *Chlamydomonas reinhardtii*. Plant Cell Physiol 51:1453–1468

Yamano T, Iguchi H, Fukuzawa H. (2013) Rapid transformation of *Chlamydomonas reinhardtii* without cell-wall removal. J Biosci Bioeng 115:691–694

Figure legends

Fig. 1 Effect of cycloheximide (CHX) on the accumulation and localization of LCIB. (A) LCIB localization after switching from light to dark. Cells harboring GFP-LCIB were acclimated to low-CO_2 (LC) conditions in the light (LC-light), followed by a shift to LC conditions in the dark (LC-dark) for 2 h, and GFP signals were observed. Arrowheads in the differential image contrast (DIC) panel indicate the pyrenoid. Bar = 5 μm. (B) Experimental conditions for examining the effect of CHX. Each number indicates the sampling time for immunoblotting analysis in (C), and arrows indicate the time points for adding 10 μg mL^{-1} CHX. HC, high CO_2. (C) Effect of CHX on accumulation of endogenous LCIB and LCIB-GFP. Accumulation of LCIB and LCIB-GFP was analyzed by protein immunoblotting analysis using an anti-LCIB antibody. The number above each lane indicates the sampling point depicted in (B). The lane 5D indicates the control loading the soluble proteins extracted from LC-grown 5D cells. (D) Effect of CHX on LCIB localization. Cells grown in LC-light conditions were transferred to LC-dark conditions and cultured for 2 h. Then, the cells were again transferred to LC-light conditions. CHX was added to the medium when the light condition was changed from light to dark. Bar = 5 μm.

Fig. 2 Schematic illustration of the mutant screening process. PCR-amplified hygromycin (hyg) resistance cassettes were introduced into host strain cells by electroporation. Transformant colonies were selected, cultured in 96-well microtiter plates under high-CO_2 (HC) conditions for 12 h, and shifted to low CO_2 (LC) conditions to induce the CO_2 concentrating mechanism (CCM). Then, fluorescence signals of each transformant were observed, and mutants showing aberrant LCIB localization were

analyzed.

Fig. 3 Aberrant localization of LCIB in *abl* mutants. Typical images of LCIB-GFP fluorescence signals in host strain cells and *abl* mutants are shown. All strains were grown in low-CO_2 conditions in the light, and LCIB-GFP fluorescence signals were observed using confocal fluorescence microscopy. Each image is placed with the flagella facing upwards on the panel. Black arrowheads indicate the pyrenoid. DIC, differential image contrast. Bar = 5 μm.

Fig. 4 Phenotype of *abl* mutants in respect to pyrenoid development. (A) Area of the pyrenoid in host strain cells and *abl* mutants. Host strain cells were grown under high-CO_2 (HC) and low-CO_2 (LC) conditions, and all *abl* mutants were grown under LC conditions. Cells were fixed and stained with $HgCl_2$ and bromophenol blue to visualize the pyrenoid clearly. (B) Histogram of number of cells vs. number of pyrenoids per cell. host strain, *abl-10*, *abl-11*, and *abl-12* cells were grown under LC conditions. Cells were fixed and stained. (C) Images of stained pyrenoids in host strain, *abl-10*, *abl-11*, and *abl-12* cells. The number of pyrenoids per cell is shown in the upper right of panel. Bar = 5 μm.

Fig. 5 Accumulation and fixation of inorganic carbon (Ci) in host strain, *abl-1*, and *abl-3* cells. Cells were grown under low-CO_2 (LC)-light conditions, and intracellular accumulation of dissolved Ci (left panel) and CO_2 fixation (right panel) during 80 sec of illumination was measured using a silicone-oil layer method. SIS; sorbitol impermeable space.

Online resource 1 Subcellular localization of endogenous LCIB and LCIC in host strain cells and *abl* mutants. Host strain cells and *abl* mutants were grown in low-CO_2 (LC) conditions, and subcellular localization of LCIB and LCIC was analyzed using an indirect immunofluorescence assay, as described previously (Yamano et al. 2010). DIC, differential image contrast. Bar = 5 μm.

Table 1. Photosynthetic parameters of *abl* mutant cells

	WT	*abl-1*	*abl-2*	*abl-3*	*abl-4*	*abl-5*	*abl-6*
Vmax [μmol O_2 $mgChl^{-1}$ h^{-1}]	168.4±22.8	159.6±4.2	142.9±3.0	138.7±3.0	109.0±18.4	161.6±20.4	175.7±0.0
$K_{1/2}$ (Ci) [μM]	50.7±7.1	281.6±34.5	43.2±2.6	670.5±39.5	15.4±0.1	47.6±3.7	31.3±3.4
	abl-7	*abl-8*	*abl-9*	*abl-10*	*abl-11*	*abl-12*	
Vmax [μmol O_2 $mgChl^{-1}$ h^{-1}]	159.5±12.6	132.6±3.5	149.8±16.0	134.4±21.1	145.2±2.9	127.5±5.4	
$K_{1/2}$ (Ci) [μM]	45.7±2.7	28.6±7.6	46.7±5.9	35.5±5.1	39.3±13.8	56.3±0.6	

Data are shown ± standard deviation, which were obtained from at least three independent experiments. Ci, inorganic carbon; V_{max}, maximum O_2-evolving activity.

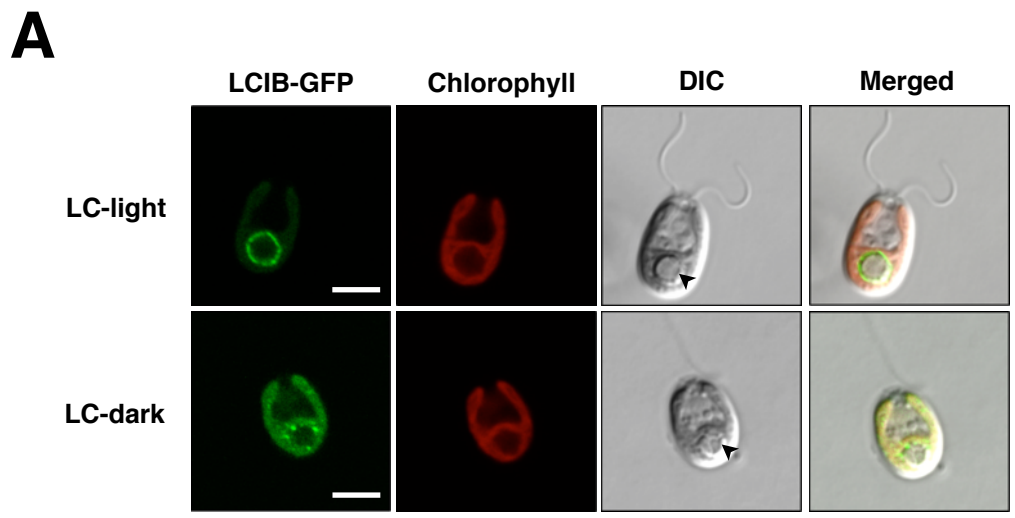

Figure 1

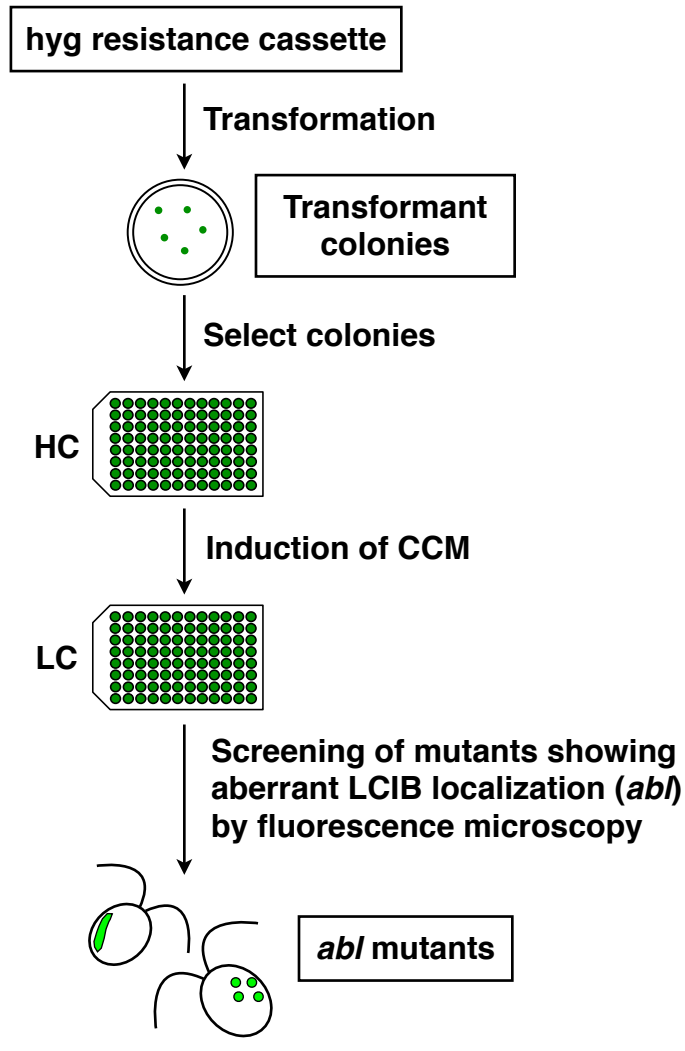

Figure 2

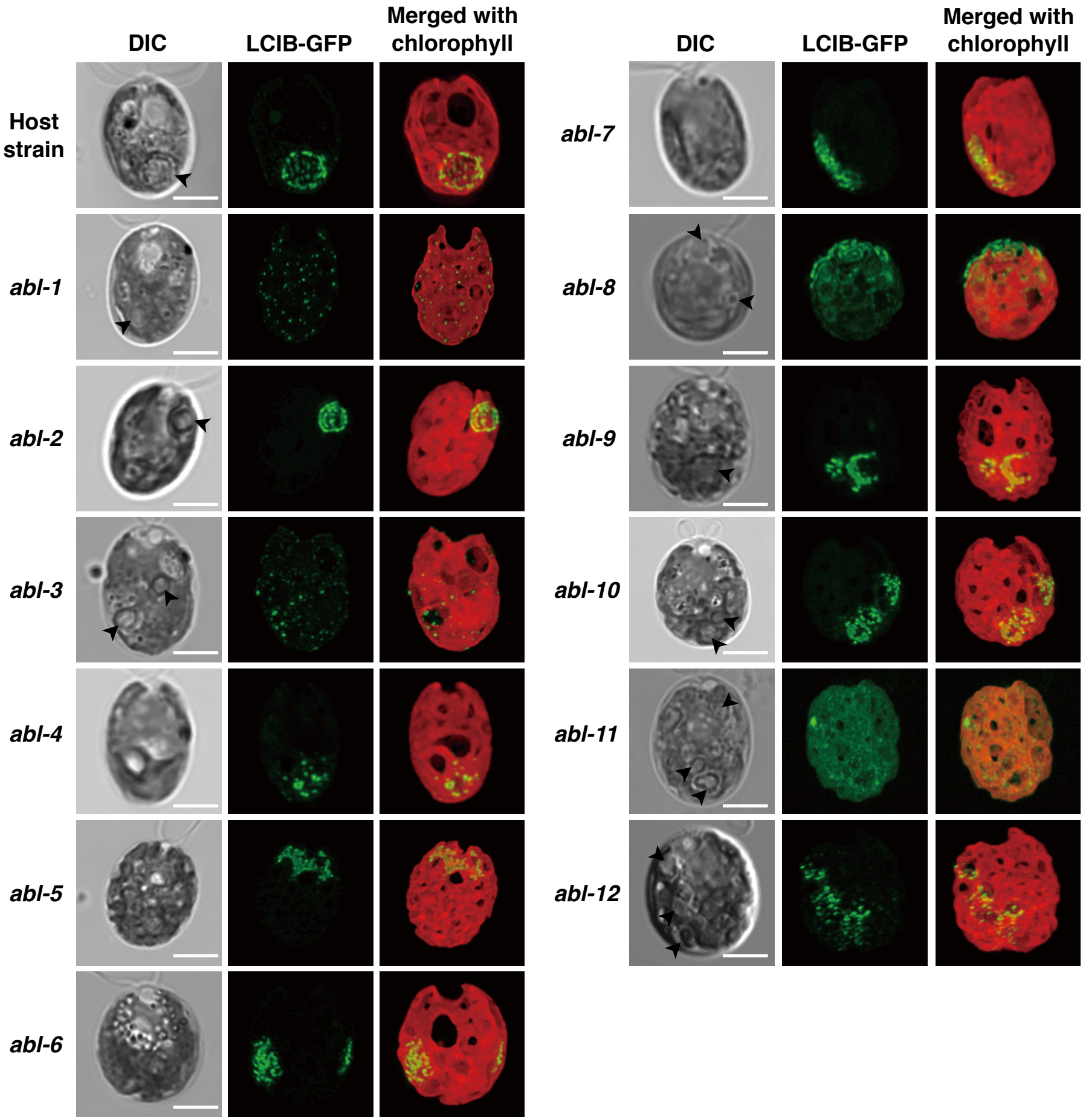

Figure 3

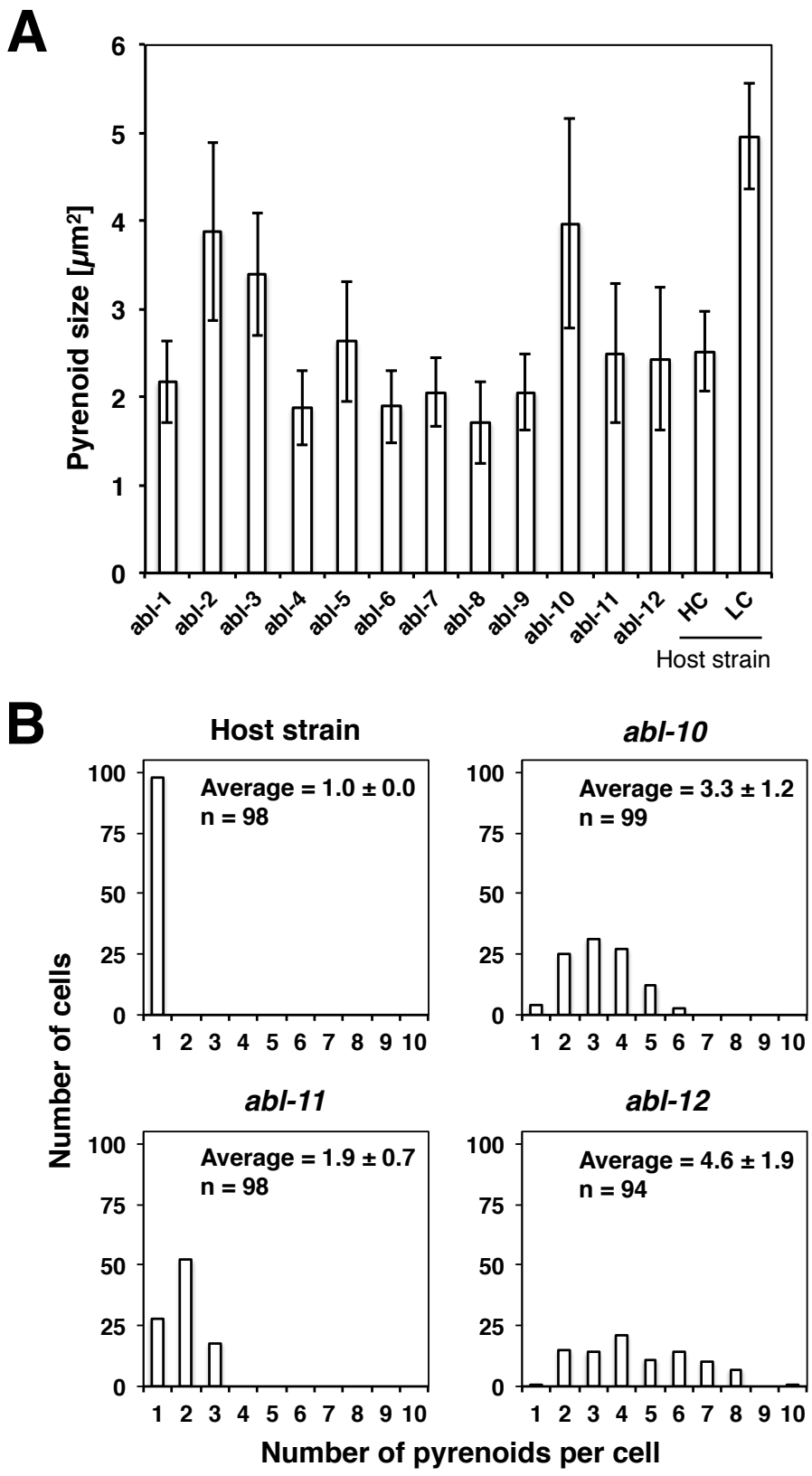

Figure 4

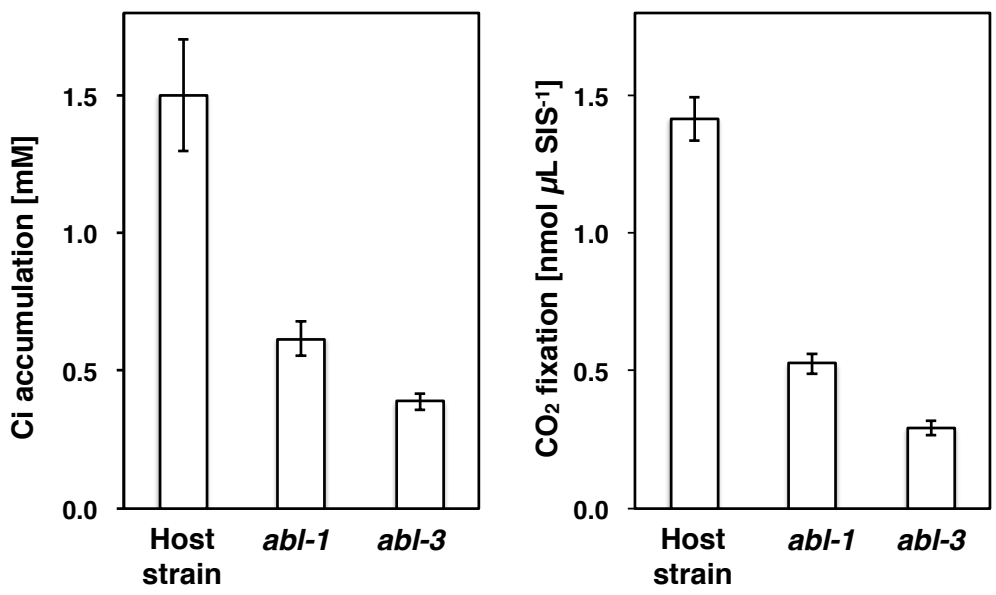

Figure 5

Supplementary material

Click to download Supplementary material: Supplemental-figure.pdf